

Production of $f_0(980)$, $f_2(1270)$ and $\phi(1020)$ in hadronic Z^0 decay

The OPAL Collaboration

Abstract

Inclusive production of the $f_0(980)$, $f_2(1270)$ and $\phi(1020)$ resonances has been studied in a sample of 4.3 million hadronic Z^0 decays from the OPAL experiment at LEP. A coupled channel analysis has been used for the f_0 in simultaneous fits to the resonances in inclusive $\pi^+\pi^-$ and K^+K^- mass spectra. Fragmentation functions are reported for the three states. Total inclusive rates are measured to be $0.141 \pm 0.007 \pm 0.011$ f_0 , $0.155 \pm 0.011 \pm 0.018$ f_2 and $0.091 \pm 0.002 \pm 0.003$ ϕ mesons per hadronic Z^0 decay. The production properties of the f_0 , including those in three-jet events, are compared with those of the f_2 and ϕ , and with the Lund string model of hadron production. All measurements are consistent with the hypothesis that the $f_0(980)$ is a conventional $q\bar{q}$ scalar meson.

Submitted to European Physical Journal C: Particles and Fields

The OPAL Collaboration

K. Ackerstaff⁸, G. Alexander²³, J. Allison¹⁶, N. Altekamp⁵, K.J. Anderson⁹, S. Anderson¹², S. Arcelli², S. Asai²⁴, S.F. Ashby¹, D. Axen²⁹, G. Azuelos^{18,a}, A.H. Ball¹⁷, E. Barberio⁸, R.J. Barlow¹⁶, R. Bartoldus³, J.R. Batley⁵, S. Baumann³, J. Bechtluft¹⁴, T. Behnke⁸, K.W. Bell²⁰, G. Bella²³, S. Bentvelsen⁸, S. Bethke¹⁴, S. Betts¹⁵, O. Biebel¹⁴, A. Biguzzi⁵, S.D. Bird¹⁶, V. Blobel²⁷, I.J. Bloodworth¹, M. Bobinski¹⁰, P. Bock¹¹, D. Bonacorsi², M. Boutemeur³⁴, S. Braibant⁸, L. Brigliadori², R.M. Brown²⁰, H.J. Burckhart⁸, C. Burgard⁸, R. Bürgin¹⁰, P. Capiluppi², R.K. Carnegie⁶, A.A. Carter¹³, J.R. Carter⁵, C.Y. Chang¹⁷, D.G. Charlton^{1,b}, D. Chrisman⁴, P.E.L. Clarke¹⁵, I. Cohen²³, J.E. Conboy¹⁵, O.C. Cooke⁸, C. Couyoumtzelis¹³, R.L. Coxe⁹, M. Cuffiani², S. Dado²², C. Dallapiccola¹⁷, G.M. Dallavalle², R. Davis³⁰, S. De Jong¹², L.A. del Pozo⁴, A. de Roeck⁸, K. Desch⁸, B. Dienes^{33,d}, M.S. Dixit⁷, M. Doucet¹⁸, E. Duchovni²⁶, G. Duckeck³⁴, I.P. Duerdoth¹⁶, D. Eatough¹⁶, P.G. Estabrooks⁶, E. Etzion²³, H.G. Evans⁹, M. Evans¹³, F. Fabbri², A. Fanfani², M. Fanti², A.A. Faust³⁰, L. Feld⁸, F. Fiedler²⁷, M. Fierro², H.M. Fischer³, I. Fleck⁸, R. Folman²⁶, D.G. Fong¹⁷, M. Foucher¹⁷, A. Fürtjes⁸, D.I. Futyan¹⁶, P. Gagnon⁷, J.W. Gary⁴, J. Gascon¹⁸, S.M. Gascon-Shotkin¹⁷, N.I. Geddes²⁰, C. Geich-Gimbel³, T. Gerasis²⁰, G. Giacomelli², P. Giacomelli⁴, R. Giacomelli², V. Gibson⁵, W.R. Gibson¹³, D.M. Gingrich^{30,a}, D. Glenzinski⁹, J. Goldberg²², M.J. Goodrick⁵, W. Gorn⁴, C. Grandi², E. Gross²⁶, J. Grunhaus²³, M. Gruwé²⁷, C. Hajdu³², G.G. Hanson¹², M. Hansroul⁸, M. Hapke¹³, C.K. Hargrove⁷, P.A. Hart⁹, C. Hartmann³, M. Hauschild⁸, C.M. Hawkes⁵, R. Hawkings²⁷, R.J. Hemingway⁶, M. Herndon¹⁷, G. Herten¹⁰, R.D. Heuer⁸, M.D. Hildreth⁸, J.C. Hill⁵, S.J. Hillier¹, P.R. Hobson²⁵, A. Hocker⁹, R.J. Homer¹, A.K. Honma^{28,a}, D. Horváth^{32,c}, K.R. Hossain³⁰, R. Howard²⁹, P. Hütemeyer²⁷, D.E. Hutchcroft⁵, P. Igo-Kemenes¹¹, D.C. Imrie²⁵, K. Ishii²⁴, A. Jawahery¹⁷, P.W. Jeffreys²⁰, H. Jeremie¹⁸, M. Jimack¹, A. Joly¹⁸, C.R. Jones⁵, M. Jones⁶, U. Jost¹¹, P. Jovanovic¹, T.R. Junk⁸, J. Kanzaki²⁴, D. Karlen⁶, V. Kartvelishvili¹⁶, K. Kawagoe²⁴, T. Kawamoto²⁴, P.I. Kayal³⁰, R.K. Keeler²⁸, R.G. Kellogg¹⁷, B.W. Kennedy²⁰, J. Kirk²⁹, A. Klier²⁶, S. Kluth⁸, T. Kobayashi²⁴, M. Kobel¹⁰, D.S. Koetke⁶, T.P. Kokott³, M. Kolrep¹⁰, S. Komamiya²⁴, R.V. Kowalewski²⁸, T. Kress¹¹, P. Krieger⁶, J. von Krogh¹¹, P. Kyberd¹³, G.D. Lafferty¹⁶, R. Lahmann¹⁷, W.P. Lai¹⁹, D. Lanske¹⁴, J. Lauber¹⁵, S.R. Lautenschlager³¹, I. Lawson²⁸, J.G. Layter⁴, D. Lazic²², A.M. Lee³¹, E. Lefebvre¹⁸, D. Lellouch²⁶, J. Letts¹², L. Levinson²⁶, B. List⁸, S.L. Lloyd¹³, F.K. Loebinger¹⁶, G.D. Long²⁸, M.J. Losty⁷, J. Ludwig¹⁰, D. Lui¹², A. Macchiolo², A. Macpherson³⁰, M. Mannelli⁸, S. Marcellini², C. Markopoulos¹³, C. Markus³, A.J. Martin¹³, J.P. Martin¹⁸, G. Martinez¹⁷, T. Mashimo²⁴, P. Mättig²⁶, W.J. McDonald³⁰, J. McKenna²⁹, E.A. Mckigney¹⁵, T.J. McMahon¹, R.A. McPherson²⁸, F. Meijers⁸, S. Menke³, F.S. Merritt⁹, H. Mes⁷, J. Meyer²⁷, A. Michelini², S. Mihara²⁴, G. Mikenberg²⁶, D.J. Miller¹⁵, A. Mincer^{22,e}, R. Mir²⁶, W. Mohr¹⁰, A. Montanari², T. Mori²⁴, S. Mihara²⁴, K. Nagai²⁶, I. Nakamura²⁴, H.A. Neal¹², B. Nellen³, R. Nisius⁸, S.W. O’Neale¹, F.G. Oakham⁷, F. Odorici², H.O. Ogren¹², A. Oh²⁷, N.J. Oldershaw¹⁶, M.J. Oreglia⁹, S. Orito²⁴, J. Pálinkás^{33,d}, G. Pásztor³², J.R. Pater¹⁶, G.N. Patrick²⁰, J. Patt¹⁰, R. Perez-Ochoa⁸, S. Petzold²⁷, P. Pfeifenschneider¹⁴, J.E. Pilcher⁹, J. Pinfold³⁰, D.E. Plane⁸, P. Poffenberger²⁸, B. Poli², A. Posthaus³, C. Rembser⁸, S. Robertson²⁸, S.A. Robins²², N. Rodning³⁰, J.M. Roney²⁸, A. Rooke¹⁵, A.M. Rossi², P. Routenburg³⁰, Y. Rozen²², K. Runge¹⁰, O. Runolfsson⁸, U. Ruppel¹⁴, D.R. Rust¹², K. Sachs¹⁰, T. Saeki²⁴, O. Sahr³⁴, W.M. Sang²⁵, E.K.G. Sarkisyan²³, C. Sbarra²⁹, A.D. Schaile³⁴, O. Schaile³⁴, F. Scharf³, P. Scharff-Hansen⁸, J. Schieck¹¹, P. Schleper¹¹, B. Schmitt⁸, S. Schmitt¹¹, A. Schönig⁸, M. Schröder⁸, M. Schumacher³, C. Schwick⁸, W.G. Scott²⁰, T.G. Shears⁸, B.C. Shen⁴, C.H. Shepherd-Themistocleous⁸,

P. Sherwood¹⁵, G.P. Siroli², A. Sittler²⁷, A. Skillman¹⁵, A. Skuja¹⁷, A.M. Smith⁸, G.A. Snow¹⁷, R. Sobie²⁸, S. Söldner-Rembold¹⁰, R.W. Springer³⁰, M. Sproston²⁰, K. Stephens¹⁶, J. Steuerer²⁷, B. Stockhausen³, K. Stoll¹⁰, D. Strom¹⁹, R. Ströhmer³⁴, P. Szymanski²⁰, R. Tafirout¹⁸, S.D. Talbot¹, P. Taras¹⁸, S. Tarem²², R. Teuscher⁸, M. Thiergen¹⁰, M.A. Thomson⁸, E. von Törne³, E. Torrence⁸, S. Towers⁶, I. Trigger¹⁸, Z. Trócsányi³³, E. Tsur²³, A.S. Turcot⁹, M.F. Turner-Watson⁸, I. Ueda²⁴, P. Utzat¹¹, R. Van Kooten¹², P. Vannerem¹⁰, M. Verzocchi¹⁰, P. Vikas¹⁸, E.H. Vokurka¹⁶, H. Voss³, F. Wäckerle¹⁰, A. Wagner²⁷, C.P. Ward⁵, D.R. Ward⁵, P.M. Watkins¹, A.T. Watson¹, N.K. Watson¹, P.S. Wells⁸, N. Wermes³, J.S. White²⁸, G.W. Wilson²⁷, J.A. Wilson¹, T.R. Wyatt¹⁶, S. Yamashita²⁴, G. Yekutieli²⁶, V. Zacek¹⁸, D. Zer-Zion⁸

¹School of Physics and Astronomy, University of Birmingham, Birmingham B15 2TT, UK

²Dipartimento di Fisica dell' Università di Bologna and INFN, I-40126 Bologna, Italy

³Physikalisches Institut, Universität Bonn, D-53115 Bonn, Germany

⁴Department of Physics, University of California, Riverside CA 92521, USA

⁵Cavendish Laboratory, Cambridge CB3 0HE, UK

⁶Ottawa-Carleton Institute for Physics, Department of Physics, Carleton University, Ottawa, Ontario K1S 5B6, Canada

⁷Centre for Research in Particle Physics, Carleton University, Ottawa, Ontario K1S 5B6, Canada

⁸CERN, European Organisation for Particle Physics, CH-1211 Geneva 23, Switzerland

⁹Enrico Fermi Institute and Department of Physics, University of Chicago, Chicago IL 60637, USA

¹⁰Fakultät für Physik, Albert Ludwigs Universität, D-79104 Freiburg, Germany

¹¹Physikalisches Institut, Universität Heidelberg, D-69120 Heidelberg, Germany

¹²Indiana University, Department of Physics, Swain Hall West 117, Bloomington IN 47405, USA

¹³Queen Mary and Westfield College, University of London, London E1 4NS, UK

¹⁴Technische Hochschule Aachen, III Physikalisches Institut, Sommerfeldstrasse 26-28, D-52056 Aachen, Germany

¹⁵University College London, London WC1E 6BT, UK

¹⁶Department of Physics, Schuster Laboratory, The University, Manchester M13 9PL, UK

¹⁷Department of Physics, University of Maryland, College Park, MD 20742, USA

¹⁸Laboratoire de Physique Nucléaire, Université de Montréal, Montréal, Quebec H3C 3J7, Canada

¹⁹University of Oregon, Department of Physics, Eugene OR 97403, USA

²⁰Rutherford Appleton Laboratory, Chilton, Didcot, Oxfordshire OX11 0QX, UK

²²Department of Physics, Technion-Israel Institute of Technology, Haifa 32000, Israel

²³Department of Physics and Astronomy, Tel Aviv University, Tel Aviv 69978, Israel

²⁴International Centre for Elementary Particle Physics and Department of Physics, University of Tokyo, Tokyo 113, and Kobe University, Kobe 657, Japan

²⁵Institute of Physical and Environmental Sciences, Brunel University, Uxbridge, Middlesex UB8 3PH, UK

²⁶Particle Physics Department, Weizmann Institute of Science, Rehovot 76100, Israel

²⁷Universität Hamburg/DESY, II Institut für Experimental Physik, Notkestrasse 85, D-22607 Hamburg, Germany

²⁸University of Victoria, Department of Physics, P O Box 3055, Victoria BC V8W 3P6, Canada

²⁹University of British Columbia, Department of Physics, Vancouver BC V6T 1Z1, Canada

³⁰University of Alberta, Department of Physics, Edmonton AB T6G 2J1, Canada

³¹Duke University, Dept of Physics, Durham, NC 27708-0305, USA

³²Research Institute for Particle and Nuclear Physics, H-1525 Budapest, P O Box 49, Hungary

³³Institute of Nuclear Research, H-4001 Debrecen, P O Box 51, Hungary

³⁴Ludwigs-Maximilians-Universität München, Sektion Physik, Am Coulombwall 1, D-85748 Garching, Germany

^a and at TRIUMF, Vancouver, Canada V6T 2A3

^b and Royal Society University Research Fellow

^c and Institute of Nuclear Research, Debrecen, Hungary

^d and Department of Experimental Physics, Lajos Kossuth University, Debrecen, Hungary

^e and Department of Physics, New York University, NY 1003, USA

1 Introduction

Inclusive production of mesons and baryons in Z^0 decay has been studied extensively [1], and the results have provided valuable input to the theory and phenomenology of parton hadronization. Production of the $f_0(980)$ is of particular interest because although it is well established experimentally as a scalar ($J^{PC} = 0^{++}$) state, its precise nature has long been uncertain. Indeed, there is still vigorous debate [2, 3] about the identity of the mesons which comprise the lowest lying scalar nonet of flavour $SU(3)$. Compared to the expectations for a conventional meson at a mass of around 1 GeV, the f_0 has a markedly small total width, a relatively large coupling to $K\bar{K}$, and a partial width to $\gamma\gamma$ which is an order of magnitude below theoretical expectation.

A number of suggestions have been made as to the nature of the f_0 . Jaffe and Johnson [4] performed a bag model calculation to suggest that it could be a “cryptoexotic” $qq\bar{q}\bar{q}$ state. Weinstein and Isgur [5], using a potential model of $qq\bar{q}\bar{q}$ states, showed that the f_0 could be explained as a loosely bound $K\bar{K}$ system, a so-called $K\bar{K}$ molecule. Gribov [6, 7] has proposed a theory of confinement in QCD, in which the f_0 plays the role of a novel “vacuum scalar” state, a bound state of a quark and antiquark with negative kinetic energy, interacting repulsively to give a state of positive total energy. Ishida et al. [8] have proposed an interpretation as a hybrid meson with a massive constituent gluon, while a scalar glueball has been suggested by Robson [9]. An analysis by Close and Amsler [10] of the scalar states suggests that the most likely candidate for the lowest-lying scalar glueball is the $f_0(1500)$; in this model, the $f_0(980)$ is a left-over state which cannot be accommodated in the scalar nonet. Lattice QCD calculations [11] also find the lightest scalar glueball mass to be around 1.5 GeV so that the glueball interpretation of the f_0 is now out of favour. Törnqvist [12], using a unitarized quark model to analyse all of the identified states in the 0^{++} sector, has concluded however that the f_0 can fit in as a conventional $q\bar{q}$ meson in the lowest 0^{++} multiplet. Similarly, an analysis by Zou and Bugg [13] of all available high-statistics $\pi^+\pi^-$ and $K\bar{K}$ scattering data concluded that the f_0 could be interpreted as a meson, and recent work by Anisovich and Sarantsev [14] has come to the same conclusion.

One aim of the present study is to look for features of f_0 production in Z^0 decay which may help to elucidate its nature. The vacuum scalar states of Gribov’s theory are expected to be compact objects with distinctive production properties, and suggestions have been made by Close et al. [7] for a number of experimental tests. In Z^0 decay, the signature would be a relatively larger yield in low multiplicity events and in events where the f_0 is isolated in rapidity. If, on the other hand, the f_0 has a significant gluonic content, its production could be enhanced in gluon jets. In contrast, if it is principally a conventional meson, its production properties may be unremarkable when compared to those of other similar states. There are presently no predictions for production rates of $qq\bar{q}\bar{q}$ states or $K\bar{K}$ molecules in Z^0 decay.

Two approaches are taken in the present analysis: a comparison of the features of f_0 production with those of two neutral isoscalar mesons, and a comparison with the JETSET 7.4 [15] implementation of the Lund string model of hadronization [16], within which the f_0 is treated as a conventional meson. The features of f_0 production are measured along with those of the $f_2(1270)$ and the $\phi(1020)$ mesons. The latter is close in mass to the f_0 , while the former is an established meson with the $q\bar{q}$ in a 3P_2 state. In the conventional meson interpretation, the f_0

would be a 3P_0 state. Since the mass difference is relatively small, the f_0 and f_2 may then be expected to have similar production properties. The Lund string model, as implemented in the JETSET 7.4 Monte Carlo program, is highly successful in describing many features of hadronic Z^0 decay events. These features include global event properties related to the perturbative phase of the initial parton shower, as well as details of the production of many different species of hadrons during the nonperturbative hadronization phase. In short, the model provides a well-tested and reliable picture of particle production in hadronic Z^0 decays [17]. Within the JETSET model, the f_0 is treated as a scalar meson composed of $u\bar{u}$ and $d\bar{d}$ pairs, and the relative production rates of 3P_0 and 3P_2 mesons are determined by a variable parameter. A comparison of the data and the results of JETSET could therefore provide information on the nature of the f_0 .

The only reported measurements of the f_0 and f_2 at LEP were made by DELPHI as part of a general study of light resonances [18] using relatively low statistics. The fragmentation functions and total rates were reported over restricted ranges of momentum. In a similar study of resonance production by ALEPH [19], the f_0 was included in fits to $\pi^+\pi^-$ mass spectra, but no rates were reported. Because the f_0 has a significant coupling to $K\bar{K}$ and peaks below threshold for this channel, its $\pi^+\pi^-$ mass spectrum will not in general exhibit the simple Breit-Wigner shape assumed in these two previous analyses. In the present study, a coupled-channel analysis is done, including $\pi^+\pi^-$ and K^+K^- data, in which proper account is taken of the opening of the $K\bar{K}$ channel in f_0 decay.

2 The OPAL detector and data samples

The OPAL detector is described in [20]. For the present analysis, the most important components were the central tracking chambers which consist of two layers of silicon microvertex detectors [21], a high-precision vertex drift chamber, a large-volume jet chamber, and a set of drift chambers (the z -chambers) which measure the coordinates of tracks along the direction of the beam. The OPAL coordinate system is defined with the z -axis following the electron beam direction; the polar angle θ is defined relative to this axis, and r and ϕ are the usual cylindrical polar coordinates. The central chambers lie within a homogeneous axial magnetic field of 0.435 T. Charged particle tracking is possible over the range $|\cos\theta| < 0.98$ for the full range of azimuthal angles. The OPAL jet chamber is capable of measuring specific energy loss, dE/dx , with a resolution, $\sigma(dE/dx)/(dE/dx)$, of 3.5% for well-reconstructed, high-momentum tracks in hadronic events [22].

The present analysis used the full OPAL sample of 4.3 million hadronic Z^0 decays recorded at LEP 1 between 1990 and 1995. To correct for losses due to the acceptance and efficiency of the experiment and the selection procedures, and also to provide signal and background shapes for fits to the data mass spectra, 6 million Monte Carlo events were used, which had been generated using JETSET 7.4 and processed through a full simulation of the experiment [23] and the data reconstruction and analysis. This ‘detector-level’ Monte Carlo sample was also used for comparison with various features of the experimental data. The JETSET version was tuned [24] using OPAL data on event shape distributions, fragmentation functions of π^\pm , K^\pm , p/\bar{p} and Λ , and LEP data on total inclusive multiplicities for 26 identified hadron species.

A detailed description of the selection of hadronic Z^0 decay events in OPAL is given in [25]. For the present analysis, tracks in the selected events were required to have: a minimum momentum transverse to the beam direction of 150 MeV/ c ; a maximum momentum of $1.07 \times E_{\text{beam}}$, based on the momentum resolution of the detector; a distance of closest approach to the interaction point less than 5 cm in the plane orthogonal to the beam direction, and the corresponding distance along the beam direction less than 40 cm; a first measured point within a radius of 75 cm from the vertex; and at least 20 hits available for measurement of specific energy loss, dE/dx .

Kaons and pions were identified using the dE/dx measurements. For each track, a χ^2 probability (weight) was formed for each of the stable particle hypotheses (e, μ , π , K and p). A track was identified as a pion or a kaon if the appropriate weight was above 5% and was larger than the weight for each of the other stable hadron hypotheses. Between momenta of 0.8 and 2.0 GeV/ c , the π , K and p bands overlap in dE/dx , leading to considerable ambiguity among hypotheses. Therefore, no tracks were identified as kaons in this momentum range although, since most particles are pions, pion identification was still allowed.

With the event and track selection cuts previously described, f_0 and f_2 decaying via $\pi^+\pi^-$ were identified with an efficiency of around 40% over the whole momentum range. The $\phi \rightarrow K^+K^-$ efficiency typically varied between 15 and 20%, although in the ϕ momentum range from 1.4 to 3.6 GeV/ c it fell below 5% because of the dE/dx cross-over region. The mass resolution at 1 GeV varied with momentum, from 15 to 20 MeV for $\pi^+\pi^-$ and from 2.5 to 4.5 MeV for K^+K^- .

3 Data analysis

3.1 Inclusive two-particle mass spectra

For simultaneous fits to $\pi^+\pi^-$ and K^+K^- mass spectra in both the real and simulated data samples, spectra were formed for inclusive $\pi^+\pi^-$, $\pi^\pm\pi^\pm$ and K^+K^- systems in bins of each of the following variables:

- scaled momentum, $x_p(= p/E_{\text{beam}})$, of the two-particle systems (nine bins)
- rapidity, y , of the two-particle systems with respect to the event thrust axis (six bins)
- rapidity gap, Δy , between the two-particle systems and the closest single charged particle (six bins)
- multiplicity, n_{ch} , of charged tracks in the event (six bins)

The last three of these variables were chosen specifically for tests of the nature of the f_0 , as discussed in section 1. To account for a large part of the combinatorial backgrounds in $\pi^+\pi^-$, mass spectra were formed by subtracting the $\pi^\pm\pi^\pm$ spectra from those for $\pi^+\pi^-$. Because the combinatorial backgrounds in K^+K^- were relatively small, and Bose-Einstein correlations could

affect the $K^{\pm}K^{\pm}$ spectra near threshold, no subtraction was done for the K^+K^- mass spectra. For the Monte Carlo sample, separate spectra were also made for the most important states contributing to the mass spectra, using information on the origin of each track at the generator level.

3.2 Selection of three-jet events

To investigate possible differences between production in quark and gluon jets, the Durham jet finder [27] was used to identify a sample of three-jet events. The cut-off value y_{cut} was set to 0.005, and the jet-finding was done using charged tracks. For each candidate three-jet event, the angle between the two lowest-energy jets was required to be greater than 30° , and in order to ensure well-reconstructed, planar events, the sum of the interjet angles was required to be larger than 358° . The jet energies were then reconstructed using the interjet angles, assuming massless kinematics. Each jet was required to contain at least two charged particles and more than 5 GeV of energy. With these cuts, 24% of all events were selected as three-jet events. Monte Carlo studies have shown that in such events, 95% of the highest-energy jets are due to quarks, while the lowest-energy jet is a gluon jet with an approximately 80% probability. Mass spectra were formed, using only tracks assigned to the same jet, in three bins of E/E_{jet} where E is the energy of the two-particle system and E_{jet} is the energy of the jet.

3.3 Fit procedures

For each bin of the above kinematic variables, the $\pi^+\pi^-$ and K^+K^- mass spectra were fitted simultaneously, using a minimum χ^2 fit, to a sum of contributions given by:

$$f(m_{\pi^+\pi^-}) = a_{f_0}^{\pi^+\pi^-} |A_{f_0}(m_{\pi\pi})|^2 + a_{f_2} \text{BW}_{f_2} + a_{\text{bgd}}^{\pi^+\pi^-} B_{\pi^+\pi^-} \quad (1)$$

$$f(m_{K^+K^-}) = a_{f_0}^{K^+K^-} |A_{f_0}(m_{KK})|^2 + a_\phi \text{BW}_\phi + a_{\text{bgd}}^{K^+K^-} B_{K^+K^-} \quad (2)$$

In equations (1) and (2), the a terms represent the intensities to be fitted, A_{f_0} is the amplitude for $f_0(980)$, BW are Breit-Wigner functions, and the B represent background functions. The a_{f_0} are related by

$$a_{f_0}^{K^+K^-} = 0.75 \frac{e_{K^+K^-}}{e_{\pi^+\pi^-}} a_{f_0}^{\pi^+\pi^-}$$

where $e_{K^+K^-}/e_{\pi^+\pi^-}$ is the ratio of the efficiency to reconstruct f_0 in K^+K^- relative to $\pi^+\pi^-$ (which varies with the bin of the kinematic variable), and the factor 0.75 comes from Clebsch-Gordan coefficients. Following Flatté [26], the coupled-channel amplitudes for $f_0(980)$ decay via $\pi\pi$ and KK were taken to be:

$$A_{f_0}(m_{\pi\pi}) = \frac{m_0 \sqrt{\Gamma_{\pi\pi}}}{m_0^2 - m_{\pi\pi}^2 - im_0(\Gamma_{\pi\pi} + \Gamma_{KK})} \quad (3)$$

$$A_{f_0}(m_{\text{KK}}) = \frac{m_0 \sqrt{\Gamma_{\text{KK}}}}{m_0^2 - m_{\text{KK}}^2 - im_0(\Gamma_{\pi\pi} + \Gamma_{\text{KK}})} \quad (4)$$

Here m_0 is the resonance mass, and the partial widths Γ are related to the coupling constants g via

$$\Gamma_{\pi\pi} = g_\pi \sqrt{\frac{m_{\pi\pi}^2}{4} - m_\pi^2} \quad \text{and} \quad \Gamma_{\text{KK}} = g_K \sqrt{\frac{m_{\text{KK}}^2}{4} - m_K^2}$$

The fact that Γ_{KK} is imaginary below KK threshold leads to distortion of the $\pi\pi$ mass spectrum from a simple Breit-Wigner shape. Interference between f_0 and $\pi^+\pi^-$ backgrounds in Z^0 decay should be negligible and was not included in the fits. In determining the meson rates, the possible presence of other f-meson resonances coupling to $\pi^+\pi^-$ has been neglected.

The experimental mass resolution was treated differently for the three states. The f_0 intensities derived from equation (3) were folded with the detector resolution separately for each bin of x_p , y , Δy , n_{ch} and E/E_{jet} . For the broad f_2 , a relativistic D-wave Breit-Wigner was used, with mass and width fixed to the Particle Data Group (PDG) values [3]. For the ϕ , where experimental mass resolution is particularly important, the shapes for the fits were taken from the detector-level output of the simulation, accounting automatically for variations of the mass resolution. The background shapes for the fits were also taken from the detector-level Monte Carlo: for $\pi^+\pi^-$, all pairs identified as $\pi^+\pi^-$ were taken, except those from the f_0 and f_2 ; and for the K^+K^- , all identified combinations were used except those due to f_0 and ϕ . In the fits, the background shapes were given additional freedom, with the $\pi^+\pi^-$ contribution multiplied by a term $(m_{\pi^+\pi^-}^{\alpha_1} + \alpha_2 m_{\pi^+\pi^-}^{\alpha_3})$ and the K^+K^- shape by $(1 + \alpha_4 m_{K^+K^-})$, with the α being variable parameters. The ρ^0 resonance in the JETSET simulation is truncated at $\pm 2.5\Gamma$; to allow for this, the ρ^0 intensity above 1.15 GeV was taken as a straight-line extrapolation from the contribution at 1.15 GeV falling to zero at 1.5 GeV.

The mass ranges of the fits were 0.82 to 1.5 GeV for $\pi^+\pi^-$, and from threshold to 1.18 GeV for K^+K^- , these limits being chosen mainly to avoid the ρ^0 peak region in $\pi^+\pi^-$ and the region of its reflection in K^+K^- (caused by particle misidentification). Figure 1 shows as an example the sum of the fitted mass spectra over the range $x_p > 0.14$, indicating clearly the signals due to the three resonances.

In fits to the total mass spectra for $x_p > 0.14$ with the f_0 parameters allowed to vary, the mass was well-constrained while the couplings g were poorly determined: $m_0 = 0.957 \pm 0.006$ GeV, $g_\pi = 0.09 \pm 0.40$ and $g_K = 0.97 \pm 0.82$. This is essentially due to the limited mass resolution and the large backgrounds in the $\pi^+\pi^-$ channel; the K^+K^- data are relatively insensitive to the f_0 parameters. The fitted mass value is in good agreement with that obtained in the high-statistics analysis made by Zou and Bugg [13] of $\pi\pi - K\bar{K}$ elastic scattering phase shifts and $\pi\pi$ and $K\bar{K}$ mass spectra from central production in pp collisions. The m_0 and g values were therefore fixed to the Zou and Bugg values, $m_0 = 0.9535$ GeV, $g_\pi = 0.111$ and $g_K = 0.423$. These couplings correspond to a branching ratio, $\text{BR}(f_0 \rightarrow \pi\pi) = 0.80$, in agreement with the PDG value. Nevertheless, there is much experimental and theoretical uncertainty in the resonance parameters appropriate for the f_0 . Indeed the PDG quotes the total width as 40 to 100 MeV. The results should therefore be taken as model-dependent measurements, which assume the Flatté parametrization with the parameter values of Zou and Bugg, and no interference with background. Fits to the $\pi^+\pi^-$ and K^+K^- spectra are shown in figures 2 and 3 for six bins of

x_p ; it can be seen from the figures that the parametrization works well in the Z^0 decay data over the entire kinematic range.

3.4 Fragmentation functions and total rates

The rates obtained from the fits in bins of x_p are given in table 1. Figure 4 shows these measured fragmentation functions, $(1/\sigma_h)d\sigma/dx_p$ (where σ_h is the total hadronic cross section), along with curves from the JETSET 7.4 Monte Carlo generator, normalized for each particle to the measured total rate seen in the data. Only statistical errors are shown for the f_0 and f_2 ; the dominant systematic errors are correlated over the x_p bins and are discussed below in section 3.5. There is clearly good agreement for all three particles between the shapes of the momentum distributions in the Monte Carlo model and those in the data.

The total inclusive rates have been measured, by integrating the fragmentation functions, to be:

$$\begin{aligned} 0.141 \pm 0.007 \pm 0.011 & f_0(980) \\ 0.155 \pm 0.011 \pm 0.018 & f_2(1270) \\ 0.091 \pm 0.002 \pm 0.003 & \phi(1020) \end{aligned}$$

per hadronic Z^0 decay. The first errors are statistical and the second systematic (discussed below). These rates compare with values of 0.154 ± 0.025 f_0 and 0.240 ± 0.061 f_2 mesons, obtained by Böhrrer [1] by extrapolating the DELPHI measurements [18] to the full range of x_p . The measurement for the ϕ is in agreement with previous OPAL [28] and DELPHI [30] results, but is three standard deviations below an ALEPH [29] measurement. The present ϕ measurement has the smallest statistical and systematic errors.

3.5 Systematic errors

Table 2 gives a summary of systematic errors on the meson rates. To estimate systematic errors for the f_0 , the uncertainties in the resonance mass and the couplings were considered. The value of m_0 was varied from 0.951 to 0.963 GeV (the range obtained when the mass was allowed to be free in the fits) while keeping the coupling constants fixed. The maximum total variation, 2.5%, was taken as the systematic error. Next m_0 and g_K were fixed and the coupling g_π was allowed to vary freely in the fit. This gave a 7% change in the total rate, which was conservatively taken as the systematic error from this source. (If, instead, the errors in the $\pi\pi$ branching ratio from the PDG are used, the systematic error would be 3%.) Finally, m_0 and g_π were fixed and g_K was allowed to vary. The f_0 rate changed by much less than the statistical error, while the ϕ rate increased by 1.5%; this was assigned as a systematic error on the ϕ measurement. Systematic errors from uncertainties in Monte Carlo modelling of the track cuts contributes 1.4% [28] for resonances decaying to two charged particles. The overall systematic error on the f_0 measurements was therefore 7.6%.

For the f_2 measurements, the main sources of systematic uncertainty also come from the resonance parametrization, although in this case it is safe to assume a normal Breit-Wigner

resonance. To take account of possible long tails in the line shape beyond the upper limit of the fits to the mass spectra, the relativistic D-wave Breit-Wigner used for the fits was integrated out to 2.2 GeV, five full widths above the nominal peak position. This resulted in an increase of 30% in the total intensity over the fitted value. Since the shape of such a resonance is uncertain so far from the pole position, one half of this extra contribution was added to each measurement of the differential cross section (the results in table 1 include these corrections), and a systematic error of $30\%/\sqrt{12}$ was assigned. The fits were repeated, varying the f_2 mass and width by one standard deviation (using the PDG values) above and below their nominal values. The maximum change in the measured rate, 6%, was assigned as a systematic error. To account for the high mass tail of the ρ^0 above 1.15 GeV, the fits were repeated assuming two extreme possibilities: the default JETSET simulation, with the shape truncated at 1.15 GeV; and a constant contribution set to the level in the simulation just below 1.15 GeV. The maximum change, 3.2%, was taken as the systematic error. With an error of 3.1% on the branching ratio to $\pi^+\pi^-$ and 1.4% from the modelling of the track cuts, the overall systematic error on the f_2 measurements was therefore 11.6%.

Systematic errors due to the simulation of the energy loss were measured by varying the assumed mean values of the theoretical dE/dx distributions for a given particle hypothesis, and the assumed resolution on the energy loss measurements. Studies of well-identified pions from K_S^0 decays, protons from Λ decays and kaons from D^0 decays were used to place limits on the maximum possible deviations of these quantities, and the analysis was repeated, with the dE/dx weights of the tracks being recalculated each time. Systematic errors were assigned as the maximum measured deviations from the standard fit values. The resulting errors were negligible for the f_0 and f_2 , and contributed a 1.3% error on the total ϕ rate. Since these errors varied with momentum, they are also given in table 1 as uncorrelated systematic errors. Because the ϕ is close to threshold, there is a small background due to conversion e^+e^- pairs, particularly at low x_p (as seen in figure 3). In the standard fit, this was included in the single background term, $B_{K^+K^-}$ of equation (2). When this component was allowed to vary independently, the total ϕ rate changed by 2%, which was taken to be the systematic error from this effect. As in [28], an error of 1% comes from uncertainty in the mass resolution and 1.4% from modelling of the track cuts. Finally an error of 1.2% was included for the $\phi \rightarrow K^+K^-$ branching ratio, bringing the overall systematic error to 3.5% (including the contribution from variation of g_K discussed above).

In all of the measurements, the possible presence of other f-meson resonances (for example the $f_0(1360)$) in the $\pi^+\pi^-$ mass spectrum has been neglected. While there is no evidence in the data for such states, and therefore no need to include them in the fits, their presence could in principle give rise to additional systematic errors, particularly for the f_2 .

3.6 Production as functions of event multiplicity and rapidity gap

As discussed in section 1, the Gribov vacuum scalar states are expected to be produced preferentially in low-multiplicity events, and when isolated in rapidity relative to the other particles. Figure 5 shows the fits to the $\pi^+\pi^-$ mass spectra in the f_0 mass region for the six bins of event charged-track multiplicity. Figure 6 gives, for each of the three resonances, the ratios of production in data relative to the detector-level JETSET sample (in which the resonances

are treated as conventional mesons) as a function of the multiplicity. Figure 7 shows the same ratios as a function of the magnitude of the rapidity difference between the resonances and the nearest charged particle. For each resonance the ratios have been normalized such that the weighted averages are unity. No evidence is seen for anomalously large production of $f_0(980)$ either at low multiplicity or at large rapidity gap, with the Monte Carlo model giving a good description. The data therefore do not provide any evidence to support the hypothesis that the f_0 is a manifestation of a vacuum scalar state.

3.7 Production in quark and gluon jets

The total rates in each of the jets in the selected three-jet events were measured by fitting to the mass spectra in the three bins of scaled energy, and summing the contributions. The jet-finding procedures described in section 3.2 were also applied to the detector-level Monte Carlo sample, and the total number of each of f_0 , f_2 and ϕ in each jet was counted. Figure 8 shows the ratios of total rates measured in the data relative to the detector-level Monte Carlo model for each of the three jet classes. The figure shows no significant evidence for any differences between production in the quark-enriched (high-energy) and the gluon-enriched (low-energy) jets.

4 Summary and conclusions

Fragmentation functions and total inclusive rates in Z^0 decay have been measured for three resonances, the $f_0(980)$, $f_2(1270)$ and $\phi(1020)$, using the full LEP 1 statistics of OPAL. The f_0 and f_2 measurements will provide input to understanding the physics of inclusive particle production in the P-wave meson sector, particularly in the context of the Monte Carlo models.

The production characteristics of the f_0 show no significant differences from those of the f_2 and ϕ mesons. In particular, the shapes of the fragmentation functions are similar for all three, and are well reproduced by the JETSET 7.4 Monte Carlo model, within which the f_0 is treated as a conventional scalar meson. The total inclusive rate for the f_0 is 0.141 ± 0.013 per hadronic Z^0 decay, similar to the value, 0.155 ± 0.021 , measured for the f_2 . The f_0 rate is significantly larger than for the ϕ , 0.091 ± 0.004 per hadronic Z^0 decay. These features are consistent with the f_0 being, like the f_2 , a $q\bar{q}$ meson in the 3P state composed mainly of $u\bar{u}$ and $d\bar{d}$.

For all three states, the production rates relative to the Monte Carlo model have been measured as functions of the charged particle multiplicity of the event and the gap in rapidity to the nearest charged particle. The distributions are found to be flat in all cases. In particular, no evidence has been found for enhanced f_0 production at low multiplicities or at large rapidity gap. There is thus no evidence to identify the f_0 with the vacuum scalar state proposed by Gribov.

Production in energy-ordered jets in three-jet events has been measured with a view to seeking differences between quark and gluon induced jets. No significant differences are seen between the data and the Monte Carlo model in the relative production rates. There is therefore no evidence for any enhanced gluon content in the f_0 .

In summary, all measured characteristics of $f_0(980)$ production in the Z^0 decay data of OPAL are consistent with its interpretation as a conventional scalar meson. Quantitative theoretical or phenomenological predictions for production of the types of states discussed in the introduction could enable more definite conclusions to be drawn from the Z^0 data.

Acknowledgements

We particularly wish to thank the SL Division for the efficient operation of the LEP accelerator at all energies and for their continuing close cooperation with our experimental group. We thank our colleagues from CEA, DAPNIA/SPP, CE-Saclay for their efforts over the years on the time-of-flight and trigger systems which we continue to use. In addition to the support staff at our own institutions we are pleased to acknowledge the Department of Energy, USA, National Science Foundation, USA, Particle Physics and Astronomy Research Council, UK, Natural Sciences and Engineering Research Council, Canada, Israel Science Foundation, administered by the Israel Academy of Science and Humanities, Minerva Gesellschaft, Benozio Center for High Energy Physics, Japanese Ministry of Education, Science and Culture (the Monbusho) and a grant under the Monbusho International Science Research Program, German Israeli Bi-national Science Foundation (GIF), Bundesministerium für Bildung, Wissenschaft, Forschung und Technologie, Germany, National Research Council of Canada, Research Corporation, USA, Hungarian Foundation for Scientific Research, OTKA T-016660, T023793 and OTKA F-023259.

References

- [1] A. Böhrer, Phys. Rep. 291 (1997) 107.
- [2] M. R. Pennigton, in Proceedings of the 6th International Conference on Hadron Spectroscopy, Ed. M. C. Birse, G. D. Lafferty and J. A. McGovern, World Scientific (1996).
- [3] Particle Data Group, R. M. Barnett al., Phys. Rev. D54 (1996) 1.
- [4] R. L. Jaffe and K. Johnson, Phys. Lett. B60 (1976) 201;
R. L. Jaffe, Phys. Rev. D15 (1977) 267 and Phys. Rev. D15 (1977) 269.
- [5] J. Weinstein and N. Isgur, Phys. Rev. D41 (1990) 2236.
- [6] V. N. Gribov, Lund preprint, LU-TP 91-7.
- [7] F. E. Close et al., Phys. Lett. B319 (1993) 291.
- [8] S. Ishida et al., in Proceedings of the 6th International Conference on Hadron Spectroscopy, Ed. M. C. Birse, G. D. Lafferty and J. A. McGovern, World Scientific (1996);
S. Ishida, H. Sawazaki, M. Oda and K. Yamada, Phys. Rev. D47 (1993) 179.
- [9] D. Robson, N. Phys. B130 (1977) 328.
- [10] C. Amsler and F. E. Close, Phys. Lett. B353 (1995) 385.
- [11] G. Bali et al., Phys. Lett. B307 (1993) 378;
D. Weingarten et al., N. Phys. B34 (1994) 29.
- [12] N. A. Törnqvist et al., Z. Phys. C68 (1995) 647.
- [13] B. S. Zou and D. V. Bugg, Phys. Rev. D48 (1993) R3948.
- [14] A. V. Anisovich and A. V. Sarantsev, Phys. Lett. B413 (1997) 137.
- [15] T. Sjöstrand, Comp. Phys. Commun. 82 (1994) 74.
- [16] B. Andersson, G. Gustafson, G. Ingelman and T. Sjöstrand, Phys. Rep. 97 (1983) 31.
- [17] I. G. Knowles and G. D. Lafferty, J. Phys. G: Nucl. Part. Phys. 23 (1997) 731.
- [18] DELPHI Coll., P. Abreu et al., Z. Phys. C65 (1994) 587.
- [19] ALEPH Coll., D. Buskulic et al., Z. Phys. C69 (1995) 379.
- [20] OPAL Coll., K. Ahmet et al., Nucl. Instrum. Methods A305 (1991) 275.
- [21] P.P. Allport et al., Nucl. Instrum. Methods A324 (1993) 34;
P.P. Allport et al., Nucl. Instrum. Methods A346 (1994) 476.
- [22] M. Hauschild et al., Nucl. Instrum. Methods A314 (1992) 74.
- [23] J. Allison et al., Nucl. Instrum. Methods A317 (1992) 47.

- [24] OPAL Coll., M.Z. Akrawy et al., Z. Phys. C47 (1990) 505;
The JETSET 7.4 parameters were tuned as described in OPAL Coll., G. Alexander et al.,
Z. Phys. C69 (1996) 543.
- [25] OPAL Coll., G. Alexander et al., Z. Phys. C5 (1991) 175.
- [26] J. B. Gay et al., Phys. Lett. 63B (1976) 220;
S. M. Flatté, Phys. Lett. 63B (1976) 224 and Phys. Lett. 63B (1976) 228.
- [27] S. Catani, Yu. L. Dokshitzer, F. Fiorani and B. R. Webber, N. Phys. B377 (1992) 445;
S. Catani et al., Phys. Lett. B269 (1991) 432;
S. Bethke, Z. Kunszt, D. E. Soper and W. J. Stirling, N. Phys. B370 (1992) 310;
N. Brown and W. J. Stirling, Z. Phys. C53 (1992) 629.
- [28] OPAL Coll., R. Akers et al., Z. Phys. C68 (1995) 1.
- [29] ALEPH Coll., D. Buskulic et al., Z. Phys. C69 (1996) 379.
- [30] DELPHI Coll., P. Abreu et al., Z. Phys. C73 (1996) 61.
- [31] G. D. Lafferty and T. R. Wyatt, Nucl. Instrum. Methods A355 (1995) 541.

x_p range	$f_0(980)$	$f_2(1270)$	$\phi(1020)$
0.00–0.06	1.04 ± 0.09	1.00 ± 0.14	$0.464 \pm 0.011 \pm 0.005$
0.06–0.12	0.57 ± 0.05	0.69 ± 0.08	$0.316 \pm 0.021 \pm 0.007$
0.12–0.14	0.30 ± 0.06	0.41 ± 0.09	$0.285 \pm 0.020 \pm 0.009$
0.14–0.16	0.20 ± 0.05	0.25 ± 0.08	$0.197 \pm 0.019 \pm 0.006$
0.16–0.20	0.21 ± 0.03	0.27 ± 0.04	$0.167 \pm 0.017 \pm 0.002$
0.20–0.25	0.13 ± 0.02	0.22 ± 0.03	$0.133 \pm 0.007 \pm 0.002$
0.25–0.35	0.085 ± 0.011	0.091 ± 0.016	$0.096 \pm 0.004 \pm 0.001$
0.35–0.50	0.046 ± 0.005	0.035 ± 0.008	$0.045 \pm 0.002 \pm 0.001$
0.50–1.00	0.0079 ± 0.0009	0.008 ± 0.001	$0.010 \pm 0.001 \pm 0.000$
0.00–1.00	0.141 ± 0.007	0.155 ± 0.011	$0.091 \pm 0.002 \pm 0.001$

Table 1: Measured differential cross sections, $(1/\sigma_h)d\sigma/dx_p$, and total inclusive rates for f_0 , f_2 and ϕ production. There are additional overall systematic errors of 7.6% for the f_0 , 11.6% for the f_2 and 3.5% for the ϕ . The uncorrelated systematic errors for the ϕ are given in the table; the error for the x_p range 0.50 – 1.00 is smaller than 0.0005. The uncorrelated systematic errors for the f_0 and f_2 are negligible in comparison with the statistical errors and the correlated systematic errors.

	$f_0(980)$	$f_2(1270)$	$\phi(1020)$
Variation of m_0	2.5%	–	–
Variation of g_π	7.0%	–	–
Variation of g_K	–	–	1.5%
f_2 resonance line shape	–	8.7%	–
f_2 mass and width	–	6.0%	–
$\text{BR}(f_2 \rightarrow \pi^+\pi^-)$	–	3.1%	–
ρ^0 resonance line shape	–	3.2%	–
dE/dx parametrization	–	–	1.3%
$\text{BR}(\phi \rightarrow K^+K^-)$	–	–	1.2%
K^+K^- mass resolution	–	–	1.0%
Photon conversions	–	–	2.0%
Track cuts	1.4%	1.4%	1.4%
Total	7.6%	11.6%	3.5%

Table 2: Sources of systematic errors on the total inclusive meson rates. Errors on the ϕ rates from uncertainties in the parametrization of dE/dx are momentum dependent, and are given in table 1 for the bins of x_p .

OPAL

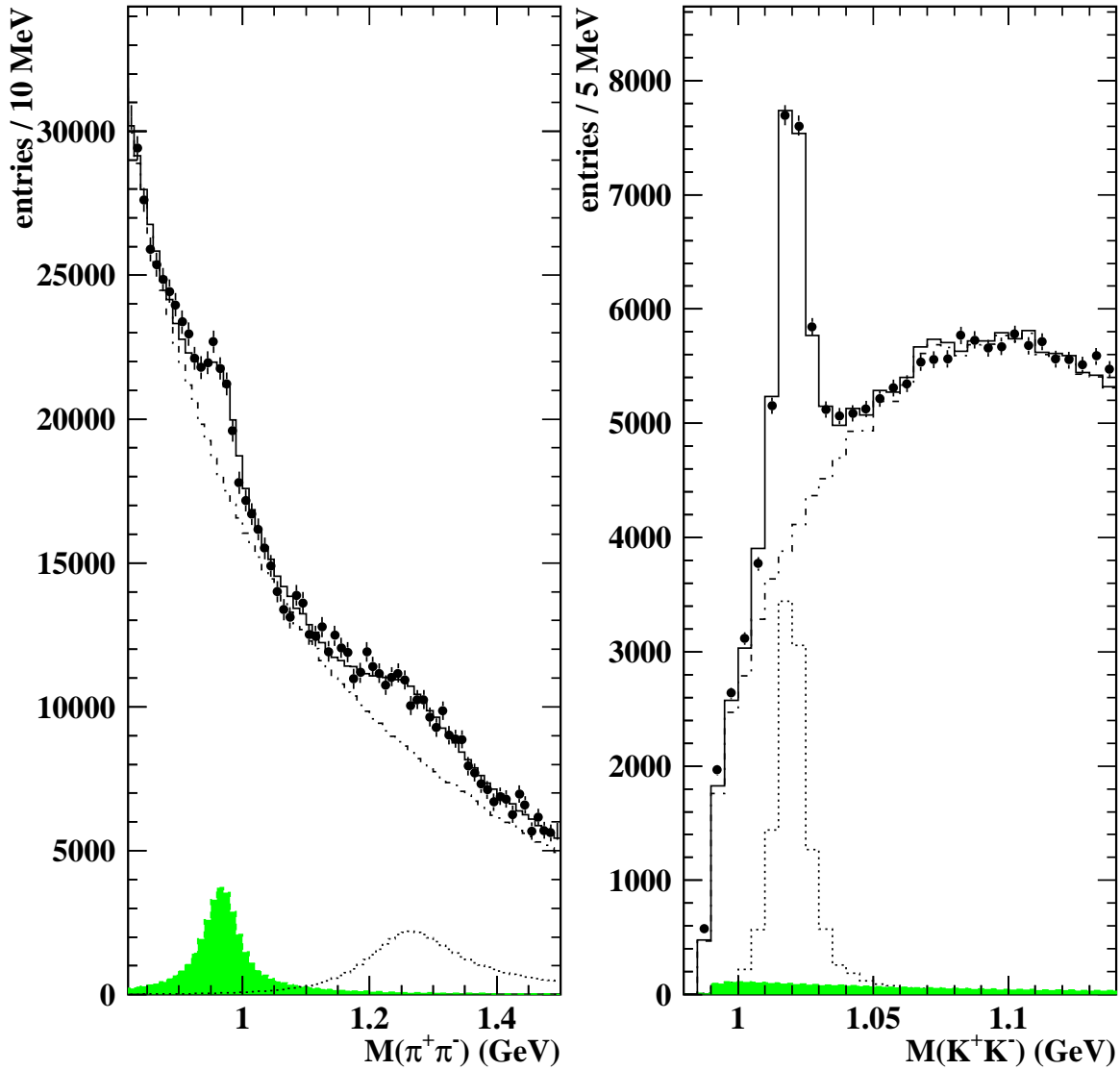


Figure 1: Sum of the fitted mass spectra of $\pi^+\pi^-$ (with like-sign spectra subtracted) and K^+K^- for $x_p > 0.14$ with the results of the fits described in the text. The points show the data, and the solid histograms give the results of the fits. The shaded histograms show the f_0 contributions, the dotted histograms give the f_2 and ϕ contributions, and the dot-dash histograms show the fitted backgrounds.

OPAL

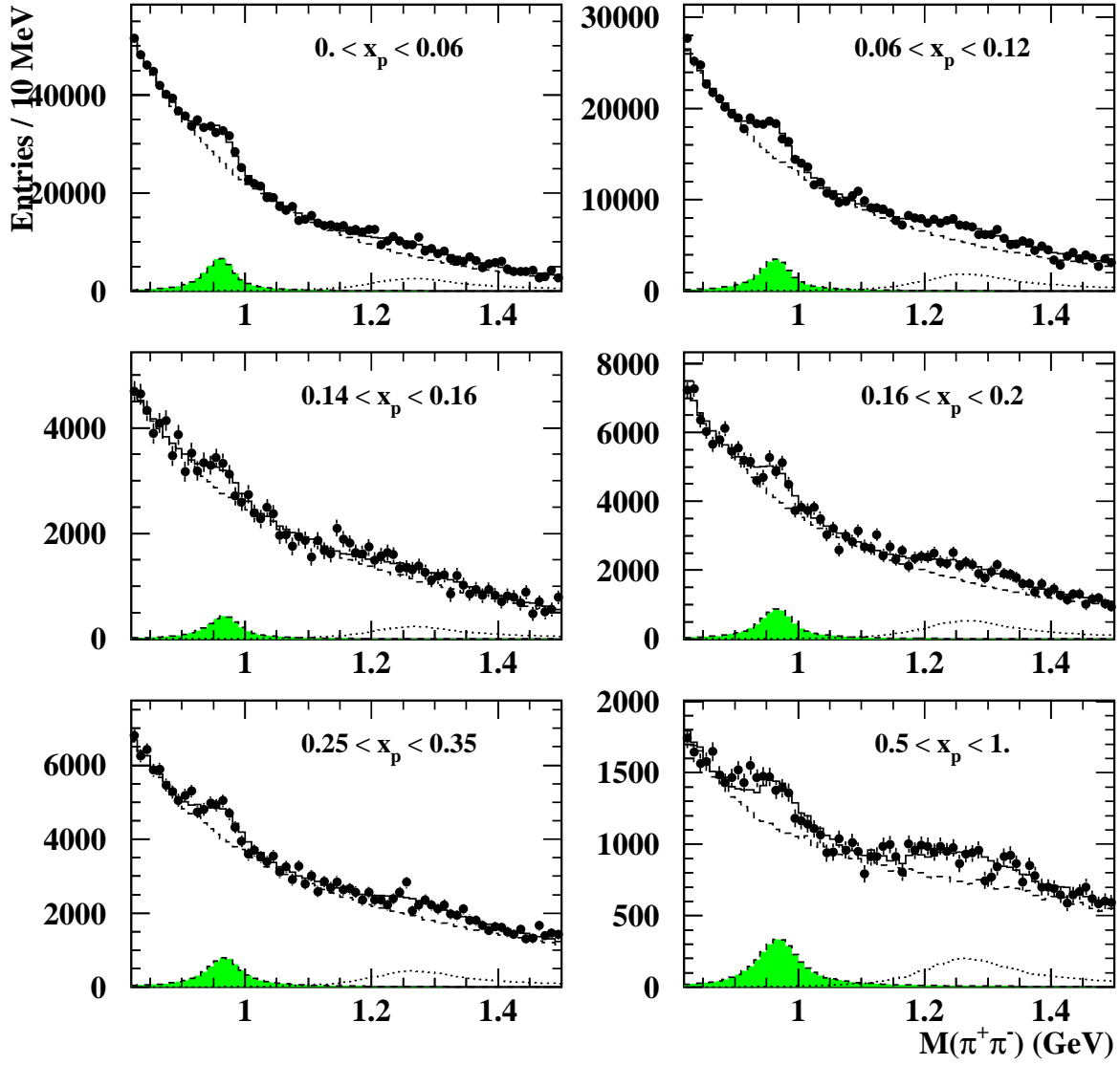


Figure 2: Mass spectra of $\pi^+\pi^-$ (with like-sign spectra subtracted) for 6 bins of x_p with the results of the fits described in the text. The points show the data, and the solid histograms give the results of the fits. The shaded histograms show the f_0 contributions, the dotted histograms show the f_2 contributions, and the dot-dash histograms show the fitted backgrounds.

OPAL

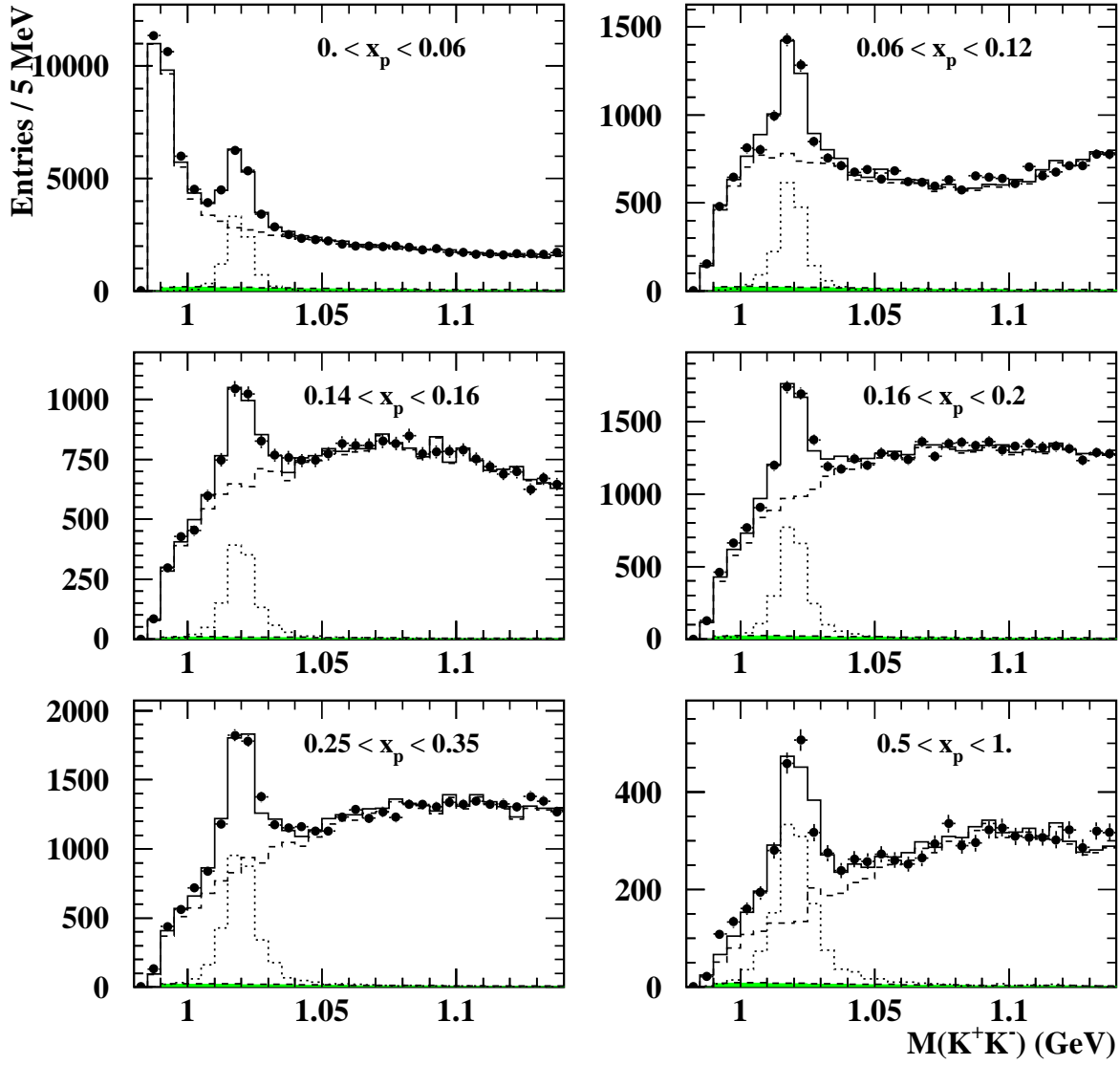


Figure 3: Mass spectra of K^+K^- for 6 bins of x_p with the results of the fits described in the text. The points show the data, and the solid histograms give the results of the fits. The shaded histograms show the f_0 contributions, the dotted histograms show the ϕ contributions, and the dot-dash histograms show the fitted backgrounds.

OPAL

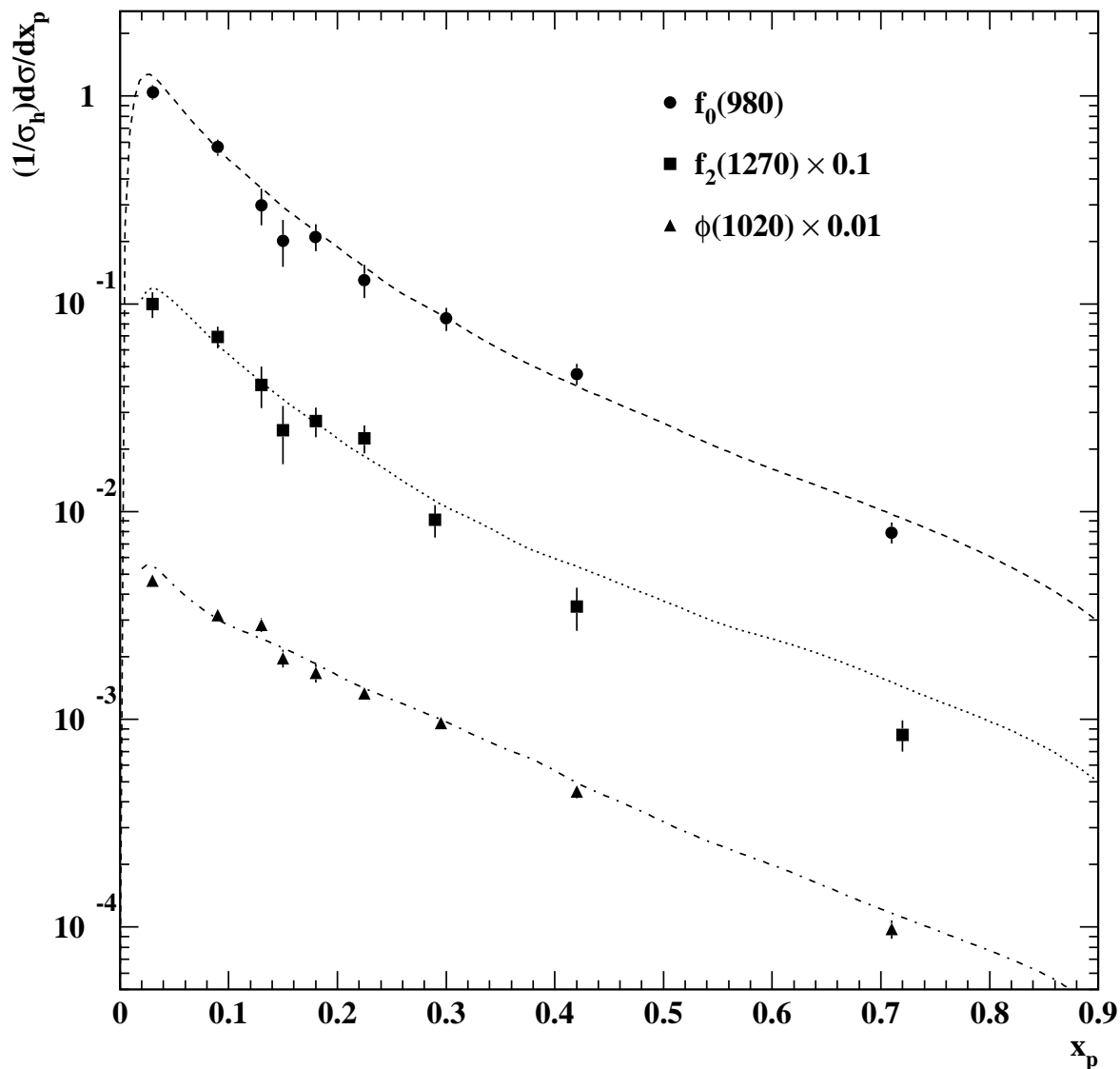


Figure 4: Measured fragmentation functions for f_0 , f_2 and ϕ together with the output of the JETSET 7.4 generator. The f_2 and ϕ measurements have been scaled by $\times 0.1$ and $\times 0.01$ respectively. The Monte Carlo curves have been normalized to the same total rate as in the data. For f_0 and f_2 , the errors are statistical only. For the ϕ , the uncorrelated systematic errors are included. There are additional, fully correlated, systematic errors of 7.6% for the f_0 , 11.6% for the f_2 and 3.5% for the ϕ . The x-coordinates for plotting the data points were evaluated following [31].

OPAL

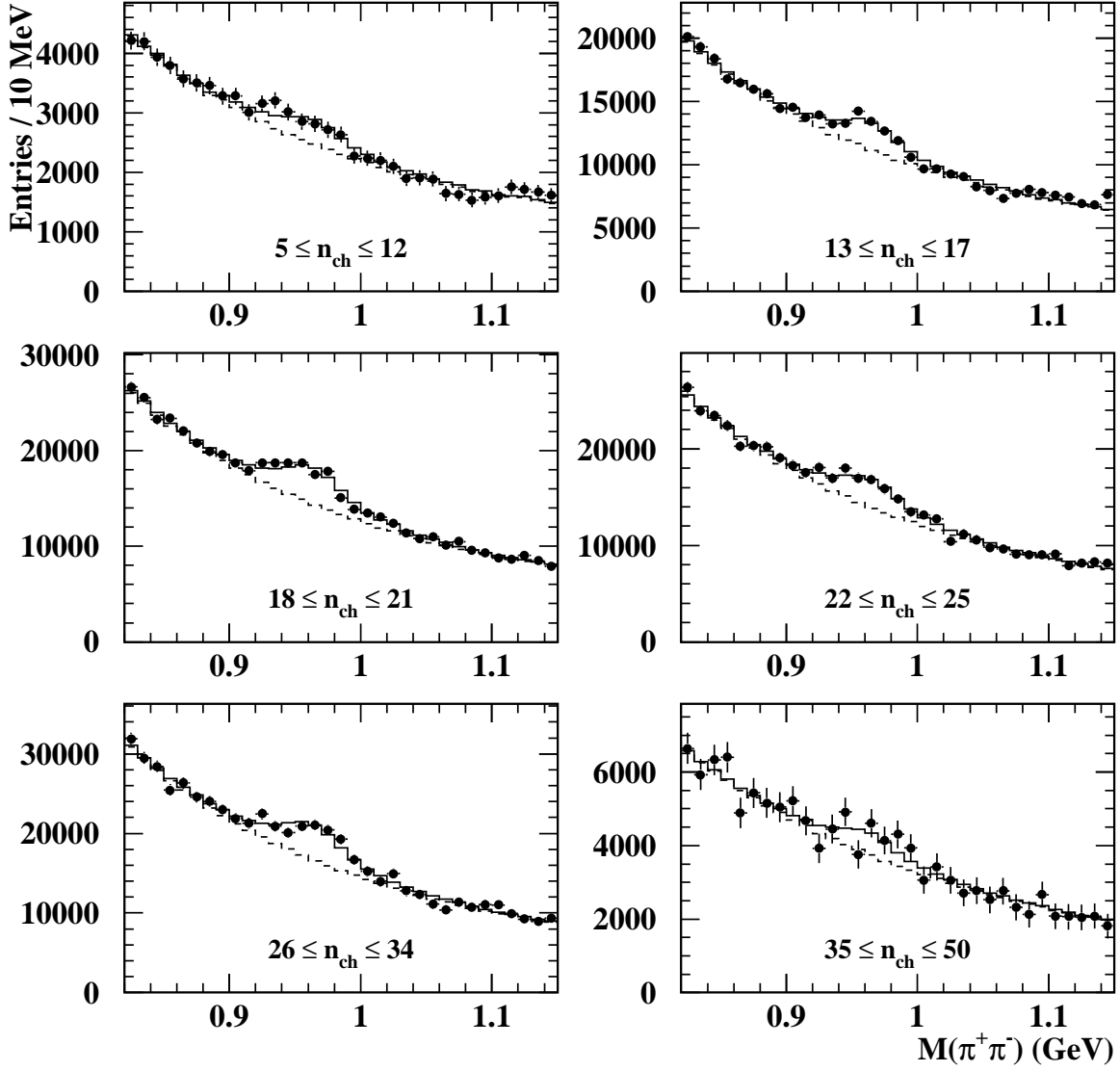


Figure 5: Fitted $\pi^+\pi^-$ spectra (with like-sign spectra subtracted) in the f_0 mass region for bins of event charged-particle multiplicity. The points show the data, and the solid histograms give the results of the fits. The dashed histograms show the fitted backgrounds.

OPAL

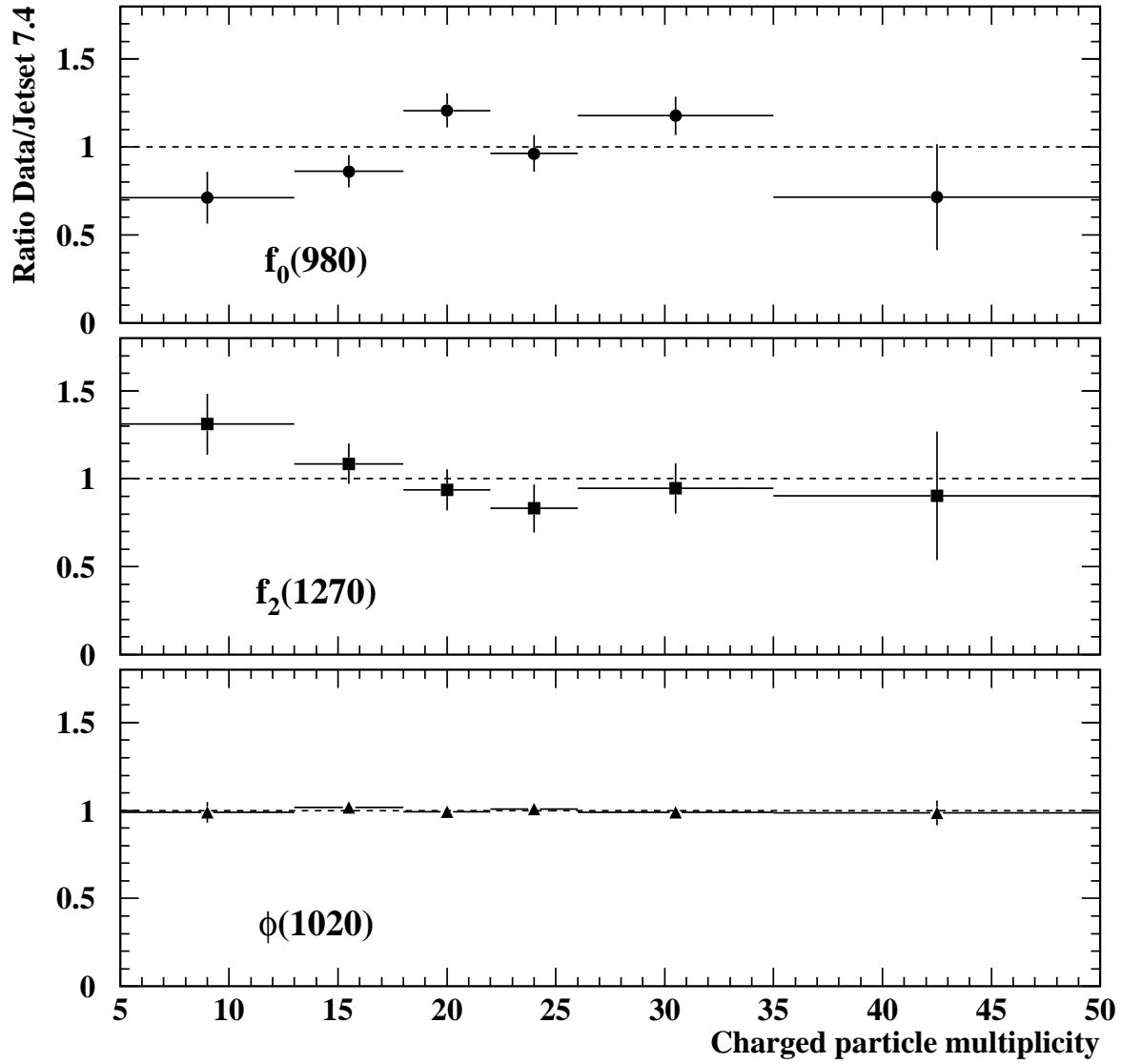


Figure 6: Ratios of production rates in data compared to the detector-level JETSET 7.4 model, for bins of event charged-particle multiplicity. The errors are statistical only. The ratios have been normalized such that the weighted average is unity for each particle.

OPAL

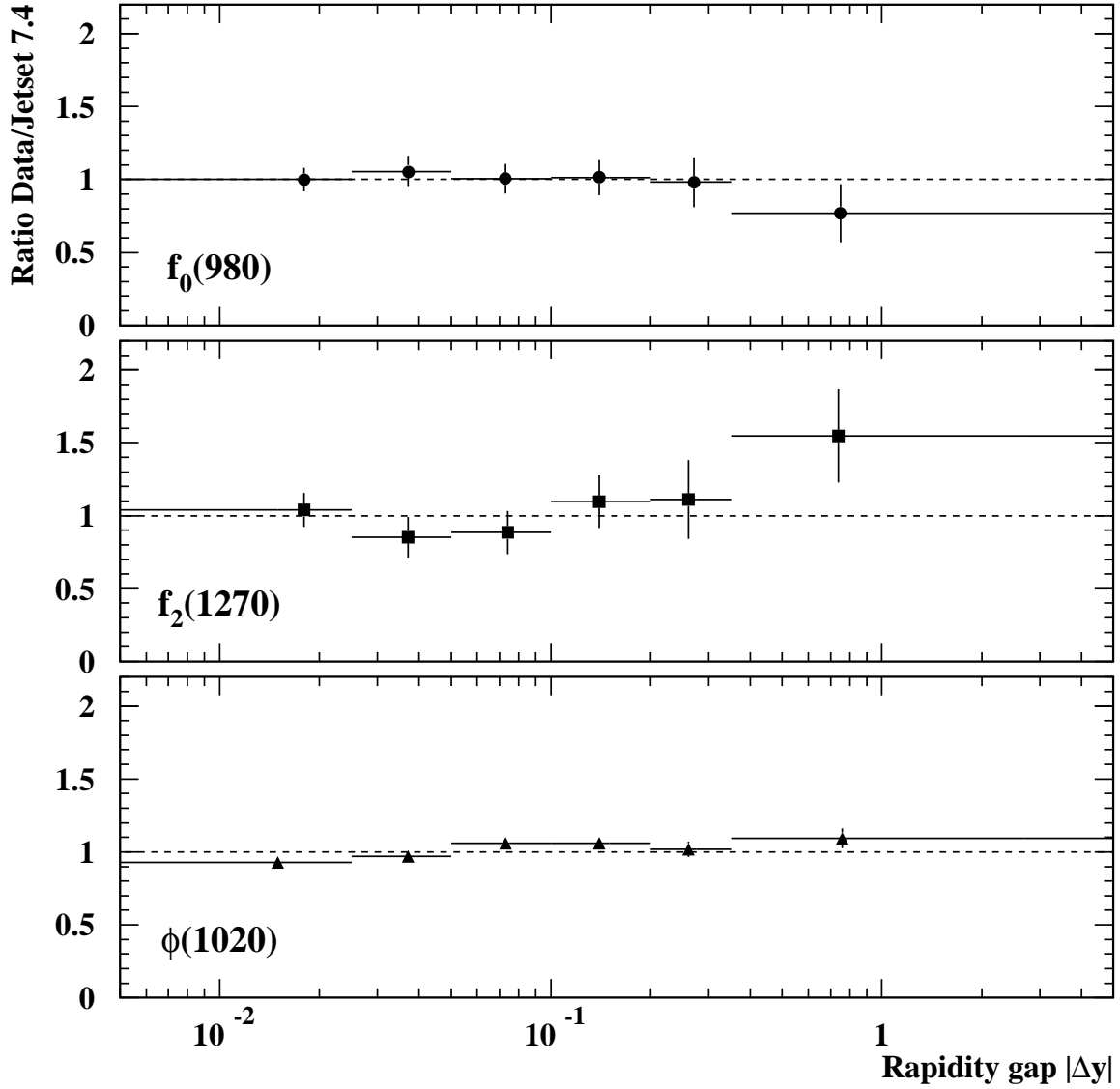


Figure 7: Ratios of total production rates in data compared to the detector-level JETSET 7.4 model, for bins of the absolute value of the rapidity difference between the meson and the nearest charged particle. The errors are statistical only. The ratios have been normalized such that the weighted average is unity for each particle. The lowest bin extends down to zero, while the highest extends to the kinematic limit.

OPAL

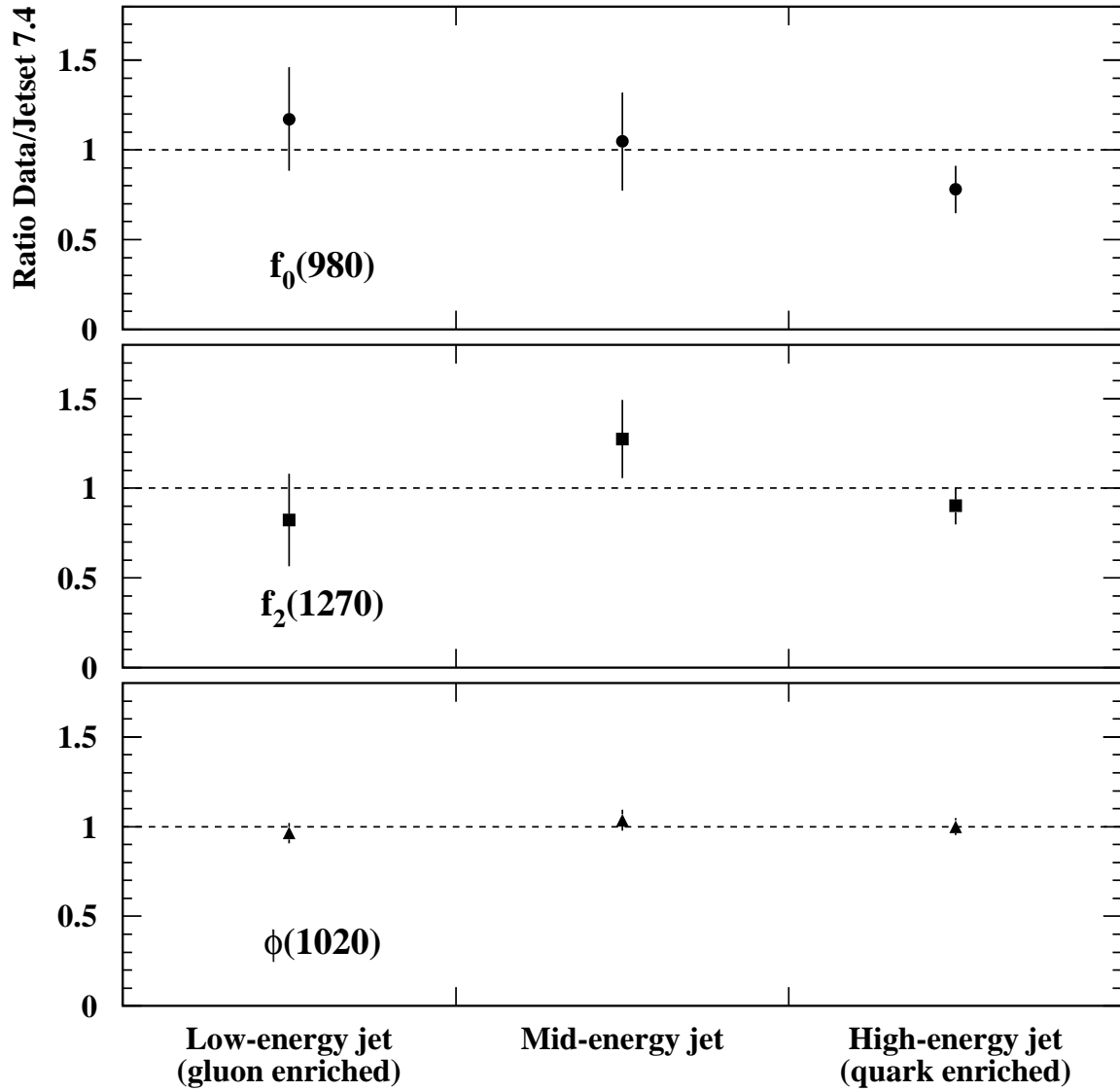


Figure 8: Ratios of total production rates in data compared to the detector-level JETSET 7.4 model for the energy-ordered jets in three-jet events. The errors are statistical only. The ratios have been normalized for each particle to give a weighted average value of unity over the three jets.